EUROPEAN COOPERATION
IN THE FIELD OF SCIENTIFIC
AND TECHNICAL RESEARCH

EURO-COST

COST 2100 TD(09) 722
Braunschweig, Germany
February, 16-18 2009

SOURCE: [1]Microwave Laboratory, Université catholique de Louvain, Louvain-la-Neuve, Belgium
[2]Forschungszentrum Telekommunikation Wien (ftw.), Vienna, Austria
[3]Smart Antennas Research Group, Stanford University, Stanford, CA, USA
[4]Eurecom Institute, Sophia-Antipolis, France

Experimental Characterization and Modeling of Outdoor-to-Indoor and Indoor-to-Indoor Distributed Channels

Claude Oestges[1], Nicolai Czink[2,3], Bernd Bandemer[3], Paolo Castiglione[2], Florian Kaltenberger[4], Arogyaswami Paulraj[3]
place du Levant, 3
1348 Louvain-la-Neuve
BELGIUM
Phone: +32 10 478098
Fax: +32 10 478705
Email: claude.oestges@uclouvain.be

Experimental Characterization and Modeling of Outdoor-to-Indoor and Indoor-to-Indoor Distributed Channels

Claude Oestges, Nicolai Czink, Bernd Bandemer, Paolo Castiglione, Florian Kaltenberger, Arogyaswami Paulraj

***Abstract*— In this report, empirical models of the outdoor-to-indoor and indoor-to-indoor distributed channels are presented. In particular, the shadowing and fading statistics are extracted from experimental data at 2.45 GHz in stationary and mobile scenarios. Highlights of the paper include a separate model for static shadowing and large-scale fading, a model for large scale fading correlation, as well as a single analytical distribution of small-scale fading for various types of indoor node mobility.**

I. Introduction

An alternative to the installation of additional base stations to increase indoor radio coverage is to establish collaboratively a reliable wireless link between a set of indoor nodes to a base station not necessarily in reach of the individual nodes. Yet, before developing algorithms tackling this challenge, the outdoor-to-indoor radio channel, as well as the channel between the co-operating nodes must be measured and modeled. The goal of the present work is to analyze outdoor-to-indoor and indoor-to-indoor distributed measured channels and to infer preliminary empirical models, for stationary and mobile indoor nodes.

Several papers have already analyzed various properties of outdoor-to-indoor and indoor-to-indoor distributed channels. In [1], a fading model for personal area networks (PANs) was derived from indoor measurements at 2.6 GHz: the main results indicate that the fading statistics are best fitted by a generalized gamma distribution, and that body shadowing should be modeled separately from environmental shadowing. In [2, 3], the outdoor-to-outdoor channel was measured for stationary receivers, and models of the Ricean K-factor were proposed. In [4], the long-term statistics of the stationary indoor channel were investigated. As far as shadowing is concerned, shadow fading correlation between a mobile terminal and several base stations (BS) or between one BS and several mobiles has been studied in [5–8]. The shadow fading correlation of distributed indoor-to-indoor channels was measured and characterized in [9, 10].

The key contributions of the present paper are as follows.

- We investigate outdoor-to-indoor (O2I) and indoor-to-indoor (I2I) distributed channels based on a wideband experimental campaign at 2.4 GHz.
- We propose a detailed statistical model of the channel, clearly separating static shadowing from time-varying fading, both large- and small-scale. Stationary as well as mobile links are considered.
- We analyze the shadowing and large-scale fading correlation properties of the indoor distributed channel.
- For mobile I2I, we propose a unique formalism to describe the small-scale fading statistics. The resulting model parameters are then related to the mobility scenario (i.e. the number of moving nodes).

Section II summarizes the experimental set-up. Section III details the general concept we use for the measurement analysis, while Section IV details the data post-processing and the estimation of propagation metrics. Sections V-A and V-B present the extracted empirical models, respectively for the outdoor-to-indoor and the indoor distributed channels. Finally, Section VI summarizes this paper and draws conclusions.

II. Experimental Set-Up

This paper is based on channel measurements of the Stanford July 2008 Radio Channel Measurement

This work was partially supported by the European Commission in the framework of the FP7 Network of Excellence in Wireless COMmunications NEWCOM++ (contract no. 216715) and by US Army grant W911NF-07-2-0027-1, and was carried out in cooperation with the European COST 2100 Action. The Telecommunications Research Center Vienna (ftw.) is supported by the Austrian Government and the City of Vienna within the competence center program COMET. The work of C. Oestges is supported by the Belgian Fonds de la Recherche Scientifique (FRS-FNRS). The work of N. Czink is supported by an Erwin Schroedinger Fellowship of the Austrian Science Fund (FWF grant number J2789-N14). The work of B. Bandemer is supported by an Eric and Illeana Benhamou Stanford Graduate Fellowship. The work of P. Castiglione is supported by the Austria Science Fund (FWF) through grant NFN SISE (S106). The work of F. Kaltenberger is supported by the European Commission in the framework of the FP7 project SENDORA (contract n. 216076) and by Eurecom.

Campaign. More details on the full campaign can be found in [11]. In this section, we briefly summarize the most important characteristics of the measurement set-up.

A. Environments

We measured two kinds of environments: O2I, downlink from a base station to distributed nodes, and I2I, between the distributed nodes.

1) Outdoor-to-Indoor: At the outdoor location, an array of two dual-polarized WiMAX base station antennas were mounted on a scissor lift raised to a height of 10 m. Regarding the indoor receivers, the 8 Rx ports of the sounder were used in two successive measurements, covering a total of 12 receive locations as represented in Figure 1, with circles and stars. The 4 receivers that are represented by stars were located at the wall close to the outdoor transmitter, and were kept at that position for the later I2I measurements. To avoid any confusion, they will be referred to as "relays" (with index 1 to 4). The indoor terminals (receivers and relays) used two different kinds of off-the-shelf vertically polarized WiFi antennas matched at 2.45 GHz. Their gain is 7dBi and 10dBi, respectively, specified in the range of 2.4-2.83 GHz. To measure the distributed radio channel jointly, we connected the antennas to the switches using long, low-loss RF cables. During the measurements, the indoor terminals were kept static, while fading was generated by walking people carrying metallic objects.

2) Indoor-to-Indoor: For the I2I segment, the measurements used the same WiFi antennas as those described above, and the same 8 (non-relay) receive locations as the O2I set-up (represented by the circles in Figure 1). The 8 Tx locations in the I2I set-up are represented by the stars (this time, the relays acted as transmitters), and the squares in Figure 1. Three types of measured scenarios are investigated:

- stationary measurements, where slow fading was generated by walking people carrying metallic objects,
- time-variant measurements, where all 8 receive antennas were moved randomly within a 2 m radius (inside a cubicle),
- time-variant measurements, where 4 Tx antennas and 4 Rx antennas were moved randomly within a 2 m radius (inside a cubicle).

Each of these scenarios was measured twice to allow for excluding measurement artifacts.

B. Measurement Equipment

The measurements were taken by means of the RUSK Stanford channel sounder at a center frequency of 2.45 GHz with a bandwidth of 240 MHz, and a test signal

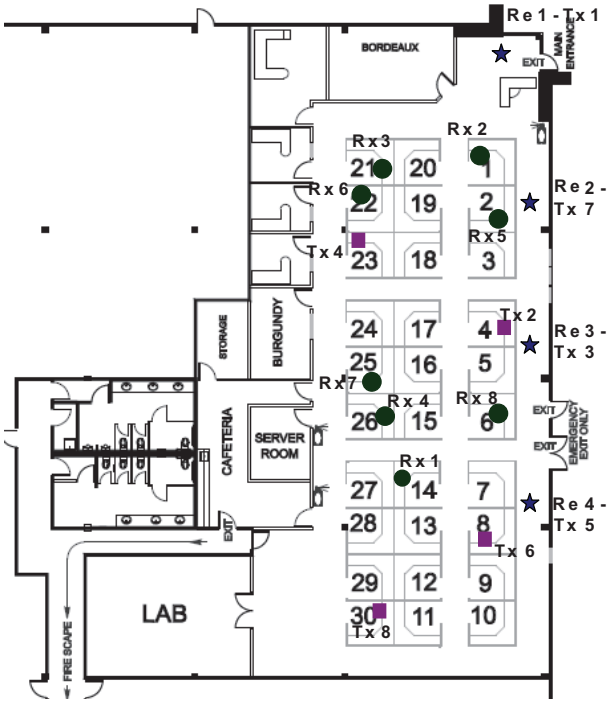

Fig. 1. Experimental set-up

length of 3.2 μs. Owing to occasional interference (e.g. from WiFi equipments and microwave ovens), the channel characterization is carried out over the lowest 70 MHz of the measured spectrum, i.e. the band from 2.33 to 2.40 GHz. Additionally, several frequencies have been removed (approximately every 10 MHz) to avoid antenna effects. Since all evaluations were done in the frequency domain only, the cutting of frequencies does not have any impact on the results.

The transmitter output power of the sounder was 0.5 W. A rubidium reference in the transmit (Tx) and receive (Rx) units ensured accurate timing and clock synchronization. The sounder used fast 1×8 switches at both transmitter and receiver, enabling switched-array MIMO channel measurements of up to 8×8 antennas, i.e. 64 links. One measurement of the whole MIMO channel at one time instant is denoted as a *block*.

The recorded frequency responses of the MIMO channels are organized in a multi-dimensional array $H[t, f, n, m]$, with dimensions time (in blocks), frequency tone, receivers, and transmitters. We had slightly different configurations for the three different scenarios, summarized in Table I.

III. General Concepts of Data Analysis

Throughout this paper, the channel coefficients are considered to reflect the superposition of the following

TABLE I
MEASUREMENT PARAMETERS USED IN THE EVALUATION

	O2I	I2I (stationary)	I2I (moving)
bandwidth	2.33 - 2.40 GHz		
number of frequency tones	200		
number of Tx antennas (M)	2 dual-polarized	8	8
number of Rx antennas (N)	8	8	8
number of blocks recorded (T)	120	120	1200
gap between blocks	250 ms	250 ms	9.83 ms
recording time	32 s	32 s	19.7 s

propagation effects:

$$\text{channel} = \text{path loss} \times \text{static shadowing} \times \times \text{large-scale fading} \times \text{small-scale fading}$$

The *path-loss* is denoted as L and is defined as the deterministic distance dependence of the received power. For given antennas, it is only a function of the transmit-to-receive distance, also known as the range. Shadowing is the combination of two processes: static shadowing and large-scale fading. *Static shadowing*, denoted as Λ, is time-invariant and represents the fact that the received powers between two links of the same range, may differ in a permanent way. For stationary scenarios, static shadowing results from the combination of two mechanisms:

- the different levels of obstruction, i.e. shadowing, of the various nodes (as an example, two receivers may be located at the same distance from the transmitter, but one receiver may be more obstructed than the other),
- the constructive or destructive combination of static multipaths, which, for a given link, causes static shadowing to possibly vary with frequency.

In mobile scenarios, only the first mechanism causes static shadowing, while both mechanisms lead to time-variant *large scale fading*. The latter, represented by the variable s, is the slow temporal variation of the received power around its mean. This variation is induced either by the large-scale motion of scatterers such as people, or by stations themselves moving throughout the environment. Finally, *small-scale fading*, denoted as r, is the classical fading behavior of the channel caused by the small-scale motions of the stations and/or the environment. The distinction between large- and small-scale fading is therefore the temporal scale of the channel variations.

Our modeling process is as follows:

1) pre-process the data in order to represent the four effects, respectively,
2) propose various statistical models which might fit the data,
3) derive estimators to extract the model parameters from these data,
4) apply these estimators to the three considered environments: (i) outdoor-to-indoor stationary distributed nodes, (ii) indoor-to-indoor stationary distributed nodes, and (iii) indoor-to-indoor moving distributed nodes,
5) build statistical models fitting the estimated data for each propagation effect.

IV. PARAMETER ESTIMATION

This section details the data processing that is used to characterize the channels.

A. Data Preprocessing

The whole frequency band is first partitioned into subbands of F_{sub} frequency tones each, leading to a total number of $B = F/F_{\text{sub}}$ subbands per time instant and link. Using subbands to increase the sample size is feasible for the stationary measurements, since the coherence bandwidth is low. In this case, we chose $F_{\text{sub}} = 5$. However, for moving measurements, the coherence bandwidth appears to be very large, hence it is not necessary to divide the whole frequency band, which is then considered as a single subband (i.e. $F_{\text{sub}} = F$). This comes to assume that the mobile channel is frequency-ergodic [12], i.e. that the large- and small-scale fading statistics over time at a given frequency are similar to the statistics over frequency at any given time. This is naturally an approximation, which seems to hold true for the measured mobile scenarios.

Regarding the indoor data, it was mentioned in Section II that two types of WiFi antennas were used. Hence, an antenna gain correction is implemented to compensate for the gain difference, so that the path losses can be rightfully compared with each other.

B. Path Loss and Static Shadowing

Let us consider the link between transmitter m and receiver n. We denote by $d = d_{nm}$ the distance between these nodes. The average received power in the b^{th}

subband is then obtained by averaging the power within the subband and over all time samples,

$$P[b,n,m] = \frac{1}{F_{\text{sub}}T}\sum_{t=1}^{T}\sum_{f=1+(b-1)F_{\text{sub}}}^{bF_{\text{sub}}}|H[t,f,n,m]|^2, \quad (1)$$

with $b = 1\dots B,\ n = 1\dots N,\ m = 1\dots M$ (remember that there is only one subband in the moving case, equal to the whole 70 MHz bandwidth).

We model path-loss and static shadowing by expressing the received power as

$$P|_{\text{dB}}(d) = P_0|_{\text{dB}} - \eta\cdot 10\log_{10}\left(\frac{d}{d_0}\right) - \Lambda|_{\text{dB}}, \quad (2)$$

where $P|_{\text{dB}}$ denotes the observed received power for a distance d between transmitter and receiver, P_0 and d_0 denote the reference power and reference distance, respectively, and the operator $|_{\text{dB}}$ denotes the conversion to dB, $P|_{\text{dB}} = 10\log_{10}P$. For I2I scenarios, d_0 is classically fixed to 1 m. The static shadowing Λ, which differs in each subband in the stationary case[1], is then defined as the difference between the observed power and the deterministic received power $P_0|_{\text{dB}} - \eta\cdot 10\log_{10}\left(d/d_0\right)$. It is a time-invariant random variable for each link and each considered subband. We define the individual path-loss L as

$$L = L_0 + \eta\cdot 10\log_{10}\left(\frac{d}{d_0}\right) + \Lambda|_{\text{dB}}, \quad (3)$$

where L_0 is the deterministic path-loss at distance d_0. The path-loss and shadowing model parameters are the so-called *path loss exponent*, η, and the standard deviation of the static shadowing, σ_Λ. The path loss exponent η is common for all links and all subbands, and is estimated by a least-square fitting using the values of $P[b,n,m]$.

C. Large-Scale Fading

Analogous to static shadowing, the time-variant large-scale fading can differ significantly in the different subbands when considering stationary scenarios. For this reason, large-scale fading is also estimated for the B subbands individually. We first average the received power over each subband for each time instant and link. Subsequently, we further average over the small-scale fading by using a moving window spanning $T_{\text{av}} = 2.6\,s$ (corresponding to either 10 samples for the stationary measurements or 160 samples for the moving measurements),

$$P_{\text{LS}}[t,b,n,m] = \frac{1}{F_{\text{sub}}T_{\text{av}}}\sum_{t'=t-T_{\text{av}}/2}^{t+T_{\text{av}}/2-1}\sum_{f=1+(b-1)F_{\text{sub}}}^{bF_{\text{sub}}}|H[t',f,n,m]|^2. \quad (4)$$

The choice of T_{av} is such that the small-scale fading is averaged out, while still following the slow variations induced by the motion of people, or by stations moving in the environment. Finally, we obtain the large-scale fading $s|_{\text{dB}}[t,b,n,m]$ as the variation of $P_{\text{LS}}|_{\text{dB}}$ around its mean,

$$s|_{\text{dB}} = P_{\text{LS}}|_{\text{dB}} - \text{E}_t\{P_{\text{LS}}|_{\text{dB}}\}, \quad (5)$$

where $\text{E}_t\{\cdot\}$ denotes the sample mean over the time axis, and the $[t,b,n,m]$ dependence is dropped to simplify the notations.

Large-scale fading is usually assumed to be log-normal distributed [13], i.e. $s|_{\text{dB}}$ is Gaussian distributed, with the standard deviation of the large-scale fading σ_s being the model parameter, which we estimate using the sample variance [14].

The large-scale fading may be correlated between different links. We estimate the correlation coefficients between links (n,m) and (n',m') by

$$C[b,n,m,n',m'] = \frac{\sum_{t=1}^{T}s|_{\text{dB}}[t,b,n,m]s|_{\text{dB}}[t,b,n',m']}{\sqrt{\sum_{t=1}^{T}s|_{\text{dB}}[t,b,n,m]^2\sum_{t=1}^{T}s|_{\text{dB}}[t,b,n',m']^2}} \quad (6)$$

These correlation coefficients are evaluated between all NM links in one measurement. The resulting $NM(NM-1)/2$ correlation values are grouped in different sets:

1) links with a common Rx (denoted as 'Rx'),
2) links with a common Tx (denoted as 'Tx'),
3) links with a common Rx or a common Tx (union of sets 1 and 2, denoted as 'Rx-Tx'),
4) links with no node in common (complement of set 3, denoted as 'disjoint'),
5) all links (union of all of sets 3 and 4, denoted as 'all').

For every such set we then calculate the mean, the standard deviation, the minimum, and the maximum value of the correlation coefficients.

D. Small-Scale Fading

small-scale fading is described by the statistics of the received signal amplitude, r. In our environment, we expect all kinds of small-scale fading, i.e. Ricean fading for strong, static links, and a smooth transition from Rayleigh fading down to Double-Rayleigh fading for moving links. A mathematically convenient method

[1]This is not the case in the moving scenarios, which is why the full bandwidth is considered as a single subband.

to approximate all three distributions — with certain limitations — is by using the Nakagami distribution.

Before estimating the different kinds of fading, we remove the effects of path-loss and shadow fading by normalizing each channel by its respective power as

$$G[t,f,n,m] = \frac{H[t,f,n,m]}{\sqrt{P_{\mathrm{LS}}[t,\lceil f/F_{\mathrm{sub}}\rceil,n,m]}}, \qquad (7)$$

where $\lceil\cdot\rceil$ is the ceiling function. The signal amplitude is then simply defined as $r = |G|$.

To estimate the statistics of r, we use as ensembles the data from all tones in each subband, and all time samples. For the stationary scenarios, we have therefore model parameter estimates for each of the considered subbands.

In the following, we discuss the different types of fading and present their parameter estimators.

1) Ricean fading: We adopt the formulation of the Ricean distribution from [15] as

$$p_{\mathrm{Rice}}(r) = \frac{r}{\sigma^2}\mathrm{e}^{-\left(\frac{r^2}{2\sigma^2}+K\right)}\mathrm{I}_0\left(r\frac{\sqrt{2K}}{\sigma}\right), \qquad (8)$$

where $\mathrm{I}_0(\cdot)$ denotes the modified Bessel function of the first kind and zero-th order, $2\sigma^2$ denotes the average power of the non-coherent part, and the K-factor describes the ratio between the powers of the coherent part and the non-coherent part of the channel.

Both K and σ^2 are estimated for every combination of Rx and Tx by numerical curve fitting to the cumulative distribution function (cdf) of the Ricean distribution. Note that if $\mathrm{E}_t\{r^2\} = 1$, then we have that σ and K are related by the following relationship: $2\sigma^2 = 1/(K+1)$.

2) Rayleigh/Double-Rayleigh fading: The Ricean fading distribution includes pure Rayleigh fading as an extreme case at $K = 0$. In some measured scenarios, however, we observe fading that is more severe than Rayleigh fading. To model this effect, we assume that the channel can be expressed as $G = w_1G_1 + w_2G_2G_3$, where G_1, G_2, G_3 are i.i.d. complex normal random variables with zero mean and unit variance. The two terms can be interpreted as a single-bounce Rayleigh-fading component and a two-bounce Double-Rayleigh-fading component, respectively. The weighting factors $w_1, w_2 > 0$ realize a tradeoff between complete Rayleigh fading ($w_2 = 0$) and complete Double-Rayleigh fading ($w_1 = 0$). Under this model, the probability density function of $r = |G|$ is (see, for example [16])

$$p_{\mathrm{RDR}}(r) = r\int_0^\infty \mathrm{e}^{-\frac{w_1^2\omega^2}{4}}\frac{4\omega}{4+w_2^2\omega^2}\,\mathrm{J}_0(r\omega)\,\mathrm{d}\omega,$$

where J_0 is the Bessel function of the first kind and zero-th order. We call this the RDR distribution.

The distribution parameters w_1 and w_2 can be estimated based on the method of moments [16] as $\hat{w}_2 = \sqrt[4]{S_4/2 - S_2^2}$ and $\hat{w}_1 = \sqrt{S_2 - \hat{w}_2^2}$, where S_i is the ith sample moment. We used these estimates as starting point for a curve fitting to the cdf of the RDR distribution, also noting that the relationship $\mathrm{E}_t\{r^2\} = 1$ is achieved when $w_1^2 + w_2^2 = 1$.

To characterize the trade-off between Rayleigh and Double-Rayleigh fading explicitly, we define $\alpha = w_2^2/(w_1^2 + w_2^2)$, so that $\alpha = 1$ is equivalent to Double-Rayleigh fading, while $\alpha = 0$ denotes pure Rayleigh fading.

3) Nakagami fading: The Nakagami-*m* distribution is given by [13]:

$$p_{\mathrm{Naka}}(r) = \frac{2}{\Gamma(m)}\left(\frac{m}{\Omega}\right)^m r^{2m-1}\mathrm{e}^{-mr^2/\Omega}, \qquad (9)$$

where Ω is the second moment, $\Gamma(\cdot)$ denotes the Gamma function and the m-parameter (sometimes denoted as shape parameter) is defined as $m = \Omega^2/\mathrm{E}\left\{\left(r^2-\Omega\right)^2\right\}$, $m \geq 0.5$.

The second moment Ω can be estimated by the unbiased maximum-likelihood estimator $\hat{\Omega} = S_2$, while the estimator of the m-parameter is the approximation of the maximum-likelihood estimator proposed in [17]. Note that $\Omega = 1$ if $\mathrm{E}_t\{r^2\} = 1$.

While the Nakagami distribution is mathematically tractable for analytical investigations, it has a number of shortcomings: (i) in contrast to the Ricean and Rayleigh/Double-Rayleigh distributions, it has no physical interpretation, (ii) for this reason, it does not fit the measurements as well, (iii) there is no analytical random-number generator for this distribution (only slow, iterative methods exist).

E. Polarization

The polarization properties of the channel could only be evaluated for the O2I links since only the outdoor base station antennas were dual-polarized.

We analyzed the combined channel-antenna depolarization, by estimating the average uplink cross-polar discrimination (XPD), defined as

$$\chi = \frac{P_{\mathrm{VV}}}{P_{\mathrm{VH}}}, \qquad (10)$$

hence, given a vertical transmitter, the XPD reflects the ratio between the average power received by the vertical transmitter, P_{VV}, and the average power received by the horizontal transmitter, P_{VH}. This ratio is calculated based on the average powers over both transmit antennas, for all subbands and all receive locations.

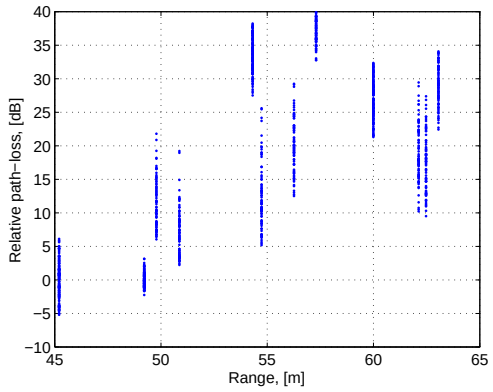

Fig. 2. Outdoor-to-indoor path loss vs. distance

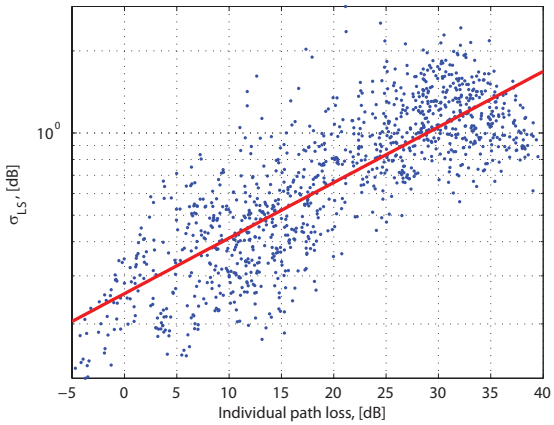

Fig. 3. Standard deviation of large-scale fading for the O2I scenario (stationary receivers).

V. Channel characterization results

A. Outdoor-to-Indoor Channels

The parameters of the Outdoor-to-Indoor (O2I) environment were extracted from all channels between the 2 (dual-polarized) Tx antennas and all 12 Rx locations (thereby including the relay nodes). The parameter estimation was carried out as described in Section IV.

1) Path loss and static shadowing: Figure 2 depicts the individual path loss of all 12 Rx nodes relative to the path loss from BS antenna 1 to relay 2. This reference link corresponds to the shortest range, and also to the best reception point in the room. The absolute path-loss L_0 of this reference link has not been measured, and is heavily dependent on the scenario. In the following, we model many fading parameters as a function of the relative path loss, $L - L_0$, instead of the absolute path loss L.

Although the path loss clearly increases with the Tx-Rx distance, a path-loss exponent can hardly be inferred as the considered scenario is too specific. Indeed, it can be observed that the path loss variation is very large over the small considered range of distances, owing to the shadowing effect of neighboring buildings for some of the Rx nodes. Additionally, O2I path-loss also includes penetration loss into the building, which was not measured. For those reasons, equation (2) is not valid in the O2I case. Similarly, shadowing cannot be estimated.

2) Large-scale fading: Regarding the large-scale fading, $s|_{\text{dB}}$, we consider its standard deviation, σ_s, which is strongly correlated with the path loss in stationary environments. Fig. 3 demonstrates that the larger the path loss, the larger the large-scale fading variations become. We model this correlation using an exponential fit

$$\log_{10}(\sigma_s) = \log_{10}(\sigma_{s,0}) + 0.02(L - L_0) + \sigma_{\sigma_s}, \quad (11)$$

where σ_{σ_s} is a zero-mean Gaussian distributed random variable with a standard deviation of 0.16.

Regarding the correlation coefficients of the large-scale fading, the mean, the standard deviation, the minimum, and the maximum value of all different subsets (cf. Sec. IV-C) are given in Table II. It can be seen that very high shadow fading correlations as well as anti-correlations occur in the measurements. When looking at all the links, the distribution of the shadow fading correlations follows a Gaussian distribution quite well (not shown). For the O2I case, the pairs of links that share a common Rx have a slightly higher correlation than the other links.

3) Small-scale fading: Given the facts that Tx and Rx nodes are all static and randomness was only introduced by people moving in the building, the fading statistics are expected to be strongly Ricean. Figure 4 represents the K-factor variation as a function of distance (upper graph) and relative path loss (lower graph).

Expectedly, the K-factor is generally very high, and decreases with increasing path loss. The variation vs. path loss is fitted by

$$K|_{\text{dB}} = K_0|_{\text{dB}} - 0.60\,(L - L_0) + \sigma_K, \quad (12)$$

where $K|_{\text{dB}}$ is the Ricean K-factor expressed in dB, and σ_K is a random variable (approximately Gaussian) of standard deviation equal to 3.8 dB. These results qualitatively confirm previous results obtained for fixed outdoor-to-outdoor channels. As an example, the decrease rate in (12) is estimated as 0.24 dB/dB in [2]. This value is smaller than our own decrease rate, but once again, we stress that our measured path loss includes a large shadowing by neighboring buildings. This explains the discrepancy.

When fitting the Nakagami distribution to the data, also large m-parameters are observed, as expected. Fig. 5 shows the m-parameter variation as a function of path

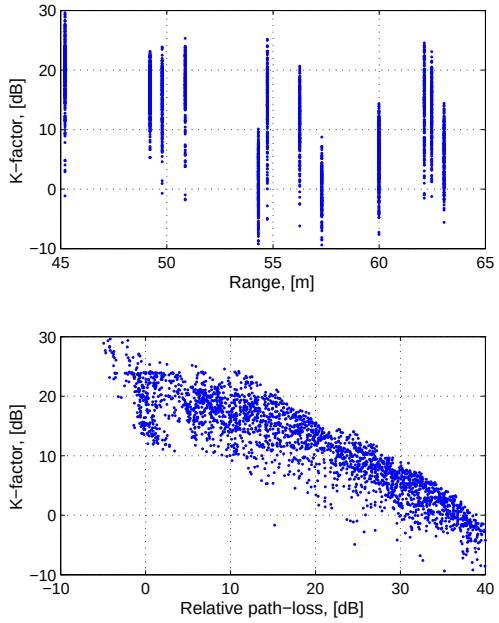

Fig. 4. K-factor vs. distance and individual relative path loss for the outdoor-to-indoor data

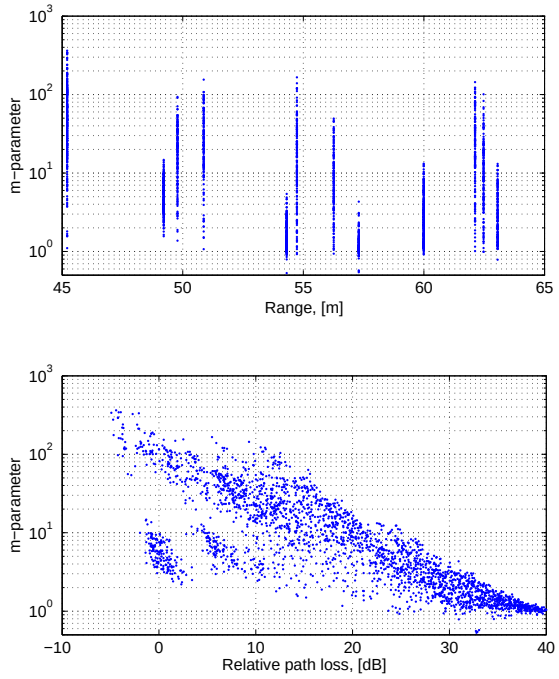

Fig. 5. Nakagami m-parameter vs. distance and individual relative path loss for the outdoor-to-indoor data

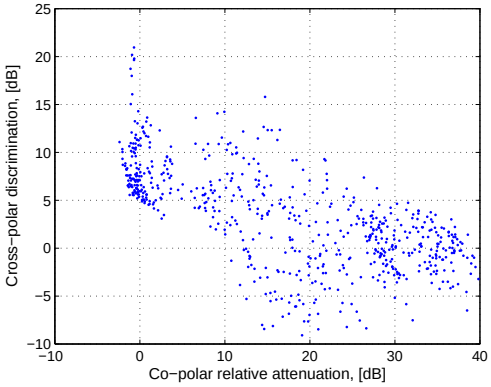

Fig. 6. Cross-polar discrimination vs. co-polar path loss

loss. The values are consistent with the observed K-factors, which is due to the close match of the Nakagami distribution to the Ricean distribution for large values of the m-parameter. For $m = 1$, the Nakagami distribution is equal to Rayleigh fading; for values $0.5 < m < 1$, the Nakagami distribution resembles fading that is worse than Rayleigh (i.e. favoring smaller amplitude values). For this reason, the scatter plot of Fig. 5 is lower bounded by the value of $m = 0.5$ (which is quite improbable in this scenario).

The variation of the m-parameter vs. path loss is also fitted by

$$\log_{10}(m) = \log_{10}(m_0) - 0.052(L - L_0) + \sigma_m \quad (13)$$

where σ_m is a random variable (approximately Gaussian) of standard deviation equal to 0.40, which is lower-bounded by $m > 0.5$.

4) Cross-polar discrimination: We evaluated the cross-polar discrimination as described in Section IV-E. Fig. 6 shows the XPD over the relative attenuation.

We find that the variation of XPD as a function of the relative attenuation $L - L_0$ is approximately linear, fitted by

$$\chi|_{\text{dB}} = \chi_0 - 0.26\,(L - L_0) + \sigma_\chi, \quad (14)$$

where σ_χ is a random approximately Gaussian variable with a standard deviation of 3.9 dB. For comparison, a decrease rate equal to 0.16 dB/dB has been evaluated in [2], with a standard deviation of 4 dB.

B. Indoor-to-Indoor Channels between Stationary Nodes

If not indicated differently, the parameters from the indoor-to-indoor channels were extracted from the distributed-nodes environment shown in Fig. 1, for all channels between the 8 transmitters and 8 receivers. The parameter estimation was carried out as described in Section IV.

Scenario	Subset	Mean	Std.	Max	Min
O2I	all	0.02	0.31	0.98	-0.89
	Rx	0.05	0.36	0.98	-0.83
	Tx	-0.02	0.29	0.81	-0.78
	Rx-Tx	0.03	0.34	0.98	-0.83
	disjoint	0.01	0.30	0.88	-0.89
I2I static	all	0.00	0.28	0.94	-0.90
	Rx	0.02	0.32	0.93	-0.90
	Tx	0.00	0.30	0.94	-0.84
	Rx-Tx	0.01	0.31	0.94	-0.90
	disjoint	0.00	0.28	0.90	-0.88
I2I moving Tx+Rx	all	0.25	0.35	0.97	-0.58
	Rx	0.30	0.37	0.82	-0.40
	Tx	0.37	0.40	0.97	-0.26
	Rx-Tx	0.34	0.38	0.97	-0.40
	disjoint	0.19	0.32	0.78	-0.58
I2I moving Rx	all	0.06	0.39	0.96	-0.91
	Rx	0.51	0.38	0.96	-0.79
	Tx	0.01	0.35	0.73	-0.83
	Rx-Tx	0.26	0.44	0.96	-0.83
	disjoint	0.01	0.35	0.86	-0.91

TABLE II
SHADOWING CORRELATION

1) Path loss and shadowing: We evaluated the relative path loss as a function of the Tx-Rx distance from the data, as highlighted in Fig. 7. From the graph, we extract the path-loss model as

$$L = L_0 + 1.75 \cdot 10 \log_{10}\left(\frac{d}{d_0}\right) + \Lambda|_{\text{dB}}, \qquad (15)$$

where $d_0 = 1\,\text{m}$, L_0 is the absolute path loss at 1 m, and the static shadowing $\Lambda|_{\text{dB}}$ is a zero-mean Gaussian distributed variable, with a standard deviation $\sigma_\Lambda = 5.85$ dB. Interestingly, the value of η is smaller than 2, which tends to indicate that waveguiding propagation effects take place.

2) Large-scale fading: For the standard deviation of the large-scale fading, we observed the same effect as in the O2I case. It is again strongly correlated with the path loss (cf. Fig. 3) and is modeled as in (11), with σ_{σ_s} being again zero-mean Gaussian distributed, but having a standard deviation of 0.22.

Regarding the large-scale fading correlation, the results are summarized in Table II. For the static scenario, it can only be noticed that all the sets show a very similar behavior and no clear relationship with the geometry of the links can be found. However, when at least one of the nodes is moving, the results look quite differently. The sets that contain the moving nodes clearly show a higher correlation than the sets that do not contain moving nodes.

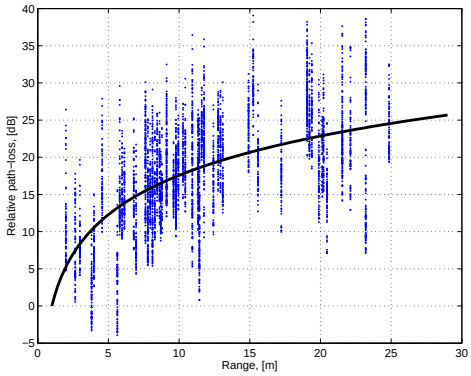

Fig. 7. Relative path loss vs. distance and linear fit of (15)

3) Small-scale fading: For stationary antennas, the channel gain is naturally found to be Ricean distributed, with the K-factor closely related to the to the Tx-Rx distance (resembling the global path loss), but also to the individual path loss, as illustrated in Fig. 8. These trends can be fitted by the following laws:

$$K|_{\text{dB}} = 16.90 - 5.25 \log_{10}\left(\frac{d}{d_0}\right) + \sigma'_K, \qquad (16)$$

where d is the Tx-Rx distance in meters, $d_0 = 1$ m and σ'_K is approximately a random Gaussian variable of deviation standard equal to 6 dB.

$$K|_{\text{dB}} = K_0|_{\text{dB}} - 0.57\,(L - L_0) + \sigma_K, \qquad (17)$$

where σ_K is a random Gaussian variable of standard deviation equal to 4.6 dB.

Similar trends are found for the Nakagami m-parameter, which is fitted by

$$\log_{10}(m) = 1.35 - 0.50 \log_{10}\left(\frac{d}{d_0}\right) + \sigma'_m \qquad (18)$$

over distance, and by

$$\log_{10}(m) = \log_{10}(m_0) - 0.053(L - L_0) + \sigma_m \qquad (19)$$

over the individual relative path loss (see Fig. 9). Variables σ'_m and σ_m are Gaussian distributed with standard deviations equal to 0.48 and 0.38, respectively. Both distributions are naturally truncated so that $m > 0.5$.

C. Indoor-to-Indoor Channels for Mobile Nodes

1) Path loss and static shadowing: Expectedly, both the path loss coefficient and the static shadowing standard deviation are similar to the stationary-node case.

2) Large-scale fading: In contrast to the stationary case, the variance of the large-scale fading, σ_s, does not depend on the path loss any more when one or

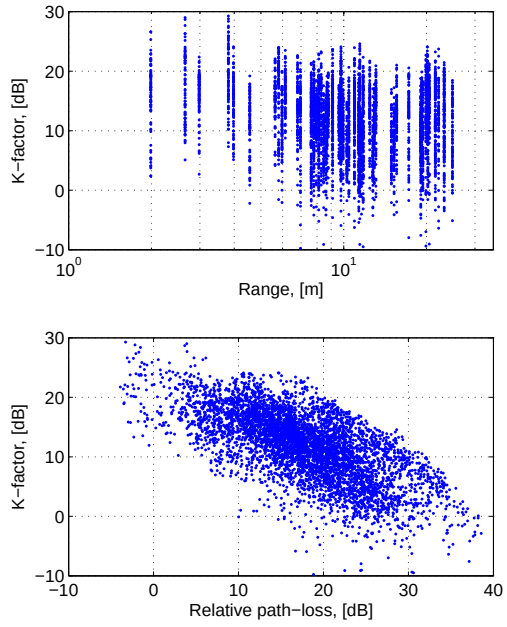

Fig. 8. K-factor vs. distance and relative path loss for the I2I stationary data

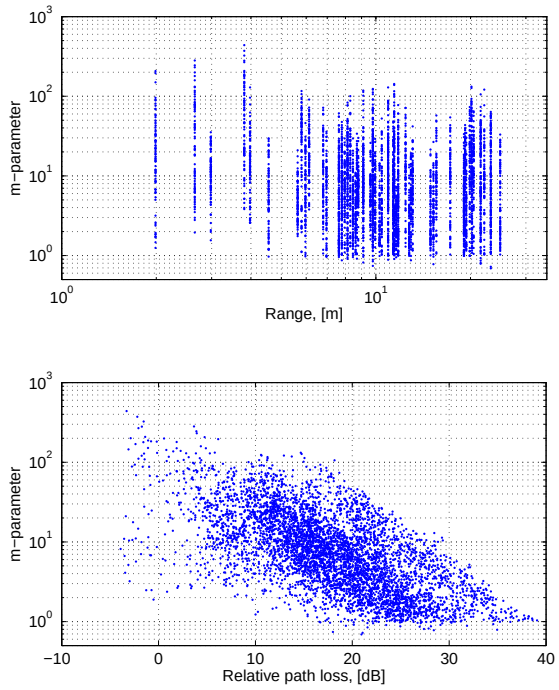

Fig. 9. Nakagami m-parameter vs. distance and relative path loss for the I2I stationary data

both stations are moving, but it is rather constant. We observed it to be similar to the static shadowing, hence we model $\sigma_s = \sigma_\Lambda$.

Table II also provides the results on the correlation coefficients. In the I2I case when at least one of the nodes is moving, it can be seen that the sets that contain the moving nodes clearly show a higher correlation than the sets that do not contain moving nodes.

3) Small-scale fading: We find that the small-scale fading statistics for this scenario vary between pure Rayleigh fading and worse-than-Rayleigh fading, i.e., fading in which smaller amplitudes are more probable than in the Rayleigh distribution. For some links, the fading even approaches the Double-Rayleigh distribution. As outlined in Section IV-D, a smooth transition between Rayleigh and below-Rayleigh distributions can be modeled by both the Nakagami distribution p_{Naka} (with $0.5 < m < 1$) and the RDR distribution p_{RDR}.

Consequently, we fit these two distributions to the small-scale fading data from the measurement. For reference purposes, the Rice distribution p_{Rice} was also fitted to the data. We normalize the small-scale fading data to satisfy $\mathrm{E}\left\{|G|^2\right\} = 1$. Correspondingly, we force each of the three distributions to satisfy this normalization exactly, i.e., we choose $\Omega = 1$ for Nakagami, $w_1^2 + w_2^2 = 1$ for RDR, and $\sigma = (2(K+1))^{-1/2}$ for the Ricean distribution. Each fitting problem then reduces to a one-dimensional optimization with respect to m, α, or K, respectively. The fitting is implemented using standard non-linear minimization algorithms, where the L_∞ norm of the CDF deviation plays the role of a goodness of fit measure (the smaller the norm, the better the fit). The optimization process is initialized by the moment-based or ML parameter estimates mentioned in Section IV-D.

In Fig. 10, the goodness of fit for the three distributions are compared to each other for all links where at least one node is moving. For $m < 1$, RDR generally achieves a better distribution fit than Nakagami. This is expected, since the RDR distribution is physically justified in these cases. For $m > 1$, not surprisingly, RDR performs worse than Nakagami or Rice. In these cases, we opt for the Rice distribution, since it is much more convenient to sample from than Nakagami.

Fig. 11 shows the best-fitting RDR distribution parameter α and the Rice K-factor over the Nakagami parameter m. As expected, lower values of m correspond to larger values of α, as fading becomes progressively worse and tends to the Double-Rayleigh case. Furthermore, for all $m < 1$, the best-fitting Rice distribution is $K = 0$, i.e., it is a pure Rayleigh distribution. Conversely, for $m > 1$, the RDR α parameter is often 0, again corresponding to pure Rayleigh, while the Rice K-factor gradually increases with m.

Therefore, the small-scale fading process can be mod-

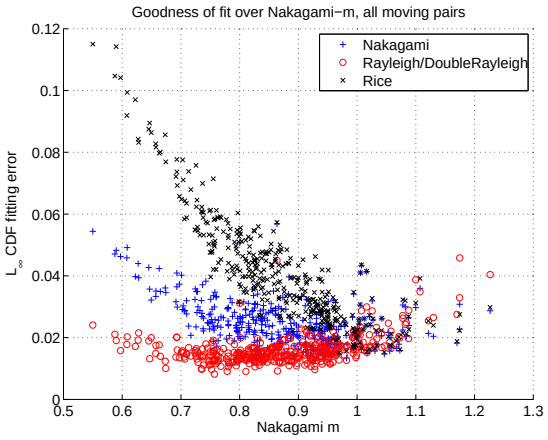

Fig. 10. Goodness of fit over Nakagami m parameter, for Nakagami, RDR, and Rice fading distributions.

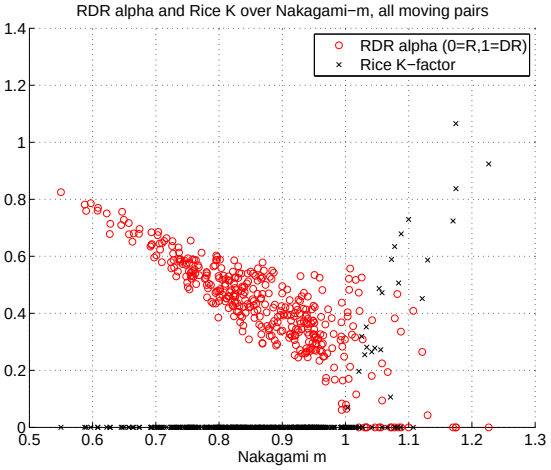

Fig. 11. RDR parameter α and Rice K-factor over Nakagami parameter m.

eled in two parts: (a) some links fade worse than Rayleigh and can be modeled by the RDR distribution, and (b) some links fade above or equal to Rayleigh and can be modeled by the Ricean distribution. In order to characterize the distribution parameters α and K for both parts, we first note that there is no discernible correlation between these parameters and the individual relative path loss $L - L_0$. Hence we take a stochastic approach. To this end, we distinguish two types of mobility: (i) either the transmitting or the receiving node is moving (*single-mobile*), and (ii) both nodes are moving (*double-mobile*).

Firstly, we conclude from the data that for double-mobile links, roughly 96.9% experience fading worse than Rayleigh fading. For single-mobile links, approximately 90.9% of all links have worse fading conditions than Rayleigh. The remaining links in each mobility setting experience fading above or equal to the Rayleigh distribution.

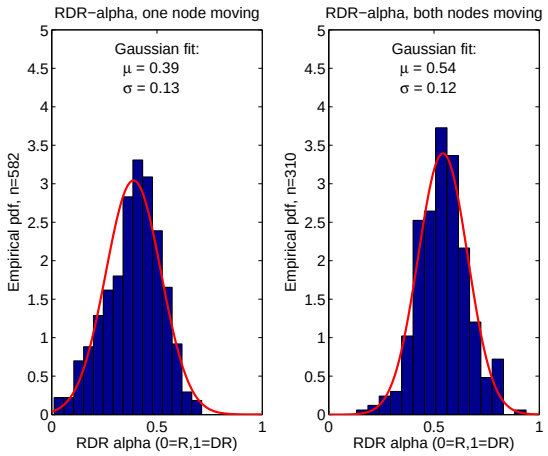

Fig. 12. RDR parameter α histogram and Gaussian fit, for single-mobile and double-mobile links.

In Fig. 12, the empirical distributions of α are shown over the ensemble of links that fade strictly below Rayleigh, separately for each type of mobility. The data suggest that a (truncated) normal distribution adequately captures the behavior. It is interesting to see that the standard deviation is approximately the same in both cases, while the mean value of α is significantly higher when both nodes are mobile. Since the number of links that fade better than Rayleigh is very low, implying a very coarse empirical PDF, we do not attempt to construct a stochastic model for the Ricean K-factor. Furthermore, among these cases, some are actually truly Rayleigh fading, whereas those that fade strictly above Rayleigh fading present a K-factor of at most 1.5 (yet, that maximum is only reached in very few cases, most cases showing K-factors between 0 and 1). Hence, we simplistically model all these Rayleigh and above-Rayleigh cases by $K = 0$, i.e., pure Rayleigh fading, which is reasonably close to Ricean fading for small K. Equivalently, we are thus modeling the above-Rayleigh or Rayleigh fading links using again the RDR distribution with $\alpha = 0$.

This allows us to express the fading of *all* links based on the RDR distribution. In summary, the distribution of α follows the law

$$\alpha_{\text{single-mobile}} \sim 0.091 \cdot \delta + 0.909 \cdot \mathcal{N}_{]0,1[}(0.39, 0.13) \tag{20}$$

$$\alpha_{\text{double-mobile}} \sim 0.031 \cdot \delta + 0.969 \cdot \mathcal{N}_{]0,1[}(0.54, 0.12), \tag{21}$$

where δ is the PDF of a random variable that is always 0, and $\mathcal{N}_{]0,1[}(\mu, \sigma)$ is a Gaussian variable of mean μ and standard deviation σ truncated in $]\,0, 1\,[$.

VI. Conclusions

This paper has presented a preliminary analysis and modeling of the outdoor-to-indoor and indoor-to-indoor channels based on experimental results. The conclusive results can be summarized as follows.

- Both outdoor-to-indoor and indoor-to-indoor distributed channels were analyzed based on a wideband experimental campaign at 2.4 GHz.
- A complete statistical model of stationary and mobile channels has been proposed, with a physically-motivated separation of static shadowing and large-scale fading, each effect being described as a log-normal variable. The standard deviation of static shadowing (in all cases) and large-scale fading (in mobile cases) is about 5.85 dB. For stationary cases, the standard deviation of large-scale fading is correlated with the relative path loss.
- We have proposed a model for the large-scale fading correlation, which enables to relate the correlation to the node mobility.
- For stationary scenarios (both O2I and I2I), small-scale fading is well approximated by a Ricean or a m-Nakagami distribution, the parameters of which being closely related to path loss (and possibly, to the distance).
- For I2I mobile transmissions, small-scale fading is modeled by a single distribution, consisting of a combination of Rayleigh and Double-Rayleigh fading. We find that the distribution is more tilted toward Double-Rayleigh when both Tx and Rx nodes are moving.

References

[1] J. Karedal, A. Johansson, F. Tufvesson, and A. Molisch, "A measurement-based fading model for wireless personal area networks," *IEEE Trans. Wireless Commun.*, vol. 7, no. 11, pp. 4575–4585, Nov. 2008.

[2] P. Soma, D. Baum, V. Erceg, R. Krishnamoorthy, and A. Paulraj, "Analysis and modeling of multiple-input multiple-output radio channels based on outdoor measurements conducted at 2.5 GHz for fixed bwa applications," in *Proc. ICC 2002 - IEEE Int. Conf. Commun.*, vol. 1, New York City, NY, May 2002, pp. 272–276.

[3] L. Ahumada, R. Feick, R. Valenzuela, and C. Morales, "Measurement and characterization of the temporal behavior of fixed wireless links," *IEEE Trans. Veh. Technol.*, vol. 54, no. 6, pp. 1913–1922, Nov. 2005.

[4] J. Medbo, J.-E. Berg, and F. Harrysson, "Temporal radio channel variations with stationary terminal," in *Proc. VTC 2004 Fall - IEEE Vehicular Technology Conf.*, vol. 1, 2004, pp. 91–95.

[5] M. Gudmundson, "Correlation model for shadow fading in mobile radio systems," *Electronics Letters*, vol. 27, no. 23, pp. 2145–2146, 7 Nov. 1991.

[6] F. Graziosi and F. Santucci, "A general correlation model for shadow fading in mobile radio systems," *IEEE Commun. Lett.*, vol. 6, no. 3, pp. 102–104, 2002.

[7] E. Perahia, D. C. Cox, and S. Ho, "Shadow fading cross correlation between basestations," in *Vehicular Technology Conference, 2001. VTC 2001 Spring. IEEE VTS 53rd*, vol. 1, 2001, pp. 313–317.

[8] J. Weitzen and T. J. Lowe, "Measurement of angular and distance correlation properties of log-normal shadowing at 1900 MHz and its application to design of PCS systems," *IEEE Trans. Veh. Technol.*, vol. 51, no. 2, pp. 265–273, 2002.

[9] P. Agrawal and N. Patwari, "Correlated link shadow fading in multi-hop wireless networks," Tech. Rep. arXiv:0804.2708, Apr 2008. [Online]. Available: http://arxiv.org/abs/0804.2708

[10] N. Patwari and P. Agrawal, "Nesh: A joint shadowing model for links in a multi-hop network," in *Proc. IEEE International Conference on Acoustics, Speech and Signal Processing (ICASSP 2008)*, Apr. 2008, pp. 2873–2876.

[11] N. Czink, B. Bandemer, G. Vazquez, A. Paulraj, and L. Jalloul, "July 2008 radio measurement campaign: Measurement documentation," Tech. Rep., July 2008.

[12] R. Kattenbach, "Statistical modeling of small-scale fading in directional channels," *IEEE J. Select. Areas Commun.*, vol. 20, no. 3, pp. 584–592, Apr. 2002.

[13] J. Parsons, *The mobile radio propagation channel*. London, UK: 2nd ed., Wiley, 2000.

[14] S. M. Kay, *Fundamentals of Statistical Signal Processing, Estimation Theory*. Prentice Hall, 1993.

[15] C. Oestges and B. Clerckx, *MIMO Wireless Communications*. Elsevier Academic Press, 2007.

[16] J. Salo, H. M. El-Sallabi, and P. Vainikainen, "Statistical analysis of the multiple scattering radio channel," *IEEE Trans. Antennas Propagat.*, vol. 54, no. 11, pp. 3114–3124, Nov. 2006.

[17] J. Cheng and N. N. Beaulieu, "Maximum-likelihood based estimation of the Nakagami m parameter," *IEEE Commun. Lett.*, vol. 5, no. 3, pp. 101–103, Mar. 2001.